Improving Cardiac Phase Extraction in IVUS Studies by Integration of Gating Methods

Gonzalo D. Maso Talou, Ignacio Larrabide, Pablo J. Blanco, Cristiano Guedes Bezerra, Pedro A. Lemos, and Raúl A. Feijóo

Abstract— Goal: **Coronary intra-vascular ultrasound (IVUS) is a fundamental imaging technique for atherosclerotic plaque assessment. However, volume-based data retrieved from IVUS studies can be misleading due to the artifacts generated by the cardiac motion, hindering diagnostic and visualization of the vessel condition. Then, we propose an image based gating method that improve the performance of the pre-existing methods, delivering a gating in an appropriate time for clinical practice.** *Methods:* **We propose a fully automatic method to synergically integrate motion signals from different gating methods to improve the cardiac phase estimation. Additionally, we present a local extrema identification method that provides a more accurate extraction of a cardiac phase and, also, a scheme for multiple phase extraction mandatory for elastography-type studies.** *Results:* **A comparison with three state-of-the-art methods is performed over 61 in-vivo IVUS studies including a wide range of physiological situations. The results show that the proposed strategy offers: (i) a more accurate cardiac phase extraction; (ii) a lower frame oversampling and/or omission in the extracted phase data (error of 1.492 ± 0.977 heartbeats per study, mean $\pm$ SD); (iii) a more accurate and robust heartbeat period detection with a Bland-Altman coefficient of reproducibility (RPC) of 0.23 sec, while the second closest method presents a RPC of 0.36 sec.** *Significance:* **The integration of motion signals performed by our method shown an improvement of the gating accuracy and reliability.**

Index Terms—Ultrasound, Gating, Motion compensation and analysis, IVUS.

I. INTRODUCTION

INTRAVASCULAR ULTRASOUND (IVUS) is a widely used imaging technique that allows a detailed description of the vessel cross-section and surrounding tissues, playing a key role in atherosclerotic plaque assessment [1]. In the case of coronary IVUS, the periodic contractions of the heart impose large displacements of the vessel structures and the acquisition probe. The estimation of volumetric measurements and axial position of structures can be misleading due to this motion [2]. Consequently, non-homogeneous displacements and rotations are observed along the axial and longitudinal directions of the vessel [3]. Since the typical IVUS study acquisition time is approximately 2 minutes, it spans along many cardiac cycles and thus, the pseudo-periodic motion imposed by the heartbeat is clearly distinguishable throughout the entire study. To deal with the motion, the heartbeat is usually divided into different cardiac phases or instants. Along the study, a repeating motion pattern is observed, which suggests a relation between each cardiac phase and the motion exerted to the structures. Several approaches explore this aspect by sampling images of a particular cardiac phase during (online) or after (offline) the IVUS acquisition [2], [4]–[15]. From these methods, a severe reduction of motion is expected, so that specific configurations of the vessel structures in a particular state of the heart can be identified.

Online ECG-gated techniques [16] use the ECG signal to acquire images of one particular cardiac phase. This procedure increases the acquisition time up to three times in comparison with the standard IVUS study [17]. Furthermore, it only presents information of one cardiac phase, neglecting all the others, forbidding studies such as palpographies or 4-D reconstructions. Online gated ECG aims at acquiring end diastolic phase images, which presents the lowest motion artifacts. However, this is difficult to achieve [2], [10]. Since the acquisition is gated in terms of R-peak offsets and due to the heart rate variability, ensuring a consistent cardiac phase acquisition is a challenging task.

To overcome these obstacles, an offline ECG gating can be performed on top of a standard IVUS study. However, the necessary equipment for this technique is not always available and, furthermore, cannot be applied retrospectively on already acquired data.

In the last decade, image-based techniques for offline gating IVUS studies have been developed [4]–[15]. As these are independent of ECG data, thay can be used at a lower cost and on already available data. As proposed in [15], these methods usually present three steps for the gating process: 1) generation of a signal that measures the cardiac motion in each frame; 2) filtering and extraction of the local extrema values from the motion signal and 3) offline gating of the study in cardiac phases. The first stage creates a signal describing the motion between neighbouring frames mentioned above. In the second step, local extrema related to a specific cardiac phase are extracted to obtain a partition of the study into cardiac cycles. Finally, each cycle is divided in cardiac phases which are used to retrieve images corresponding to a specific cardiac phase along the whole study. The main differences

G.D. Maso Talou, P.J. Blanco and R. A. Feijóo are with the National Laboratory for Scientific Computing (LNCC) and the National Institute of Science and Technology in Medicine Assisted by Scientific Computing (INCT/MACC), Petrópolis, RJ, 25651-075, Brazil e-mail: gonzalot@lncc.br.

C. Guedes Bezerra and P. A. Lemos are with Department of Interventional Cardiology, Heart Institute (InCor) and the University of São Paulo Medical School, São Paulo, SP, 05403-904, Brazil.

I. Larrabide is with the National Scientific and Technical Research Council (CONICET-Pladema), UNICEN, Tandil, BA, Argentina.

among these methods resides in the methodological strategies involved in the first two steps.

For the first step, the signal generation can be performed by analysing the lumen morphological variations [6], [7] or the image intensity features [4], [5], [8]–[15]. The methods in the former category require the segmentation of the luminal area, which is still an open research topic, and some approximations are time consuming [6]. Also, luminal topological variations, such as bifurcations, induce spurious extremal values in the motion signal.

For methods in the latter category, a set of features are used to measure the variations between adjacent images: cross-correlation [5], [9], [10], [12], sum of squared distances (SSD) [14], local mean variation [4], [11], [12], [15], Gabor filters' descriptors [8] or radial blurring [13]. It is worth noting that the blurring feature measures the motion by perturbations over the transducer probe being not sensitive to topological variations, while features like cross-correlation or SSD measure by differences between adjacent frames. Then, these features are potentially complementary to assess the motion in each frame.

The second stage frequently involves the application of a bandpass filter centered in a fundamental frequency associated with the mean cardiac frequency along the study. This strategy neglects the high order frequencies of the motion signal, which might misalign local extrema.

In the present work, we propose an automatic gating method for synergical combination of image features. Also, a novel method for phase extraction is presented using an iterative signal reconstruction scheme. Specifically, the proposed method, hereafter referred to Combined Correlation and Blurring (CCB), is based on: (i) the definition of a combined motion signal that integrates the signals presented in [10] and [13] giving less sensitivity to topological variations and a more accurate cardiac phase extraction; (ii) a scheme for the identification of local extrema in the motion signal based on the progressive incorporation of harmonic components, which increasingly refines the position of extremal values; and (iii) a physiological criteria for the extraction of multiple phases. The method validation is conducted using 61 in-vivo IVUS studies from 21 patients including a wide range of functional and physiological situations (different degrees of stenoses, stent deployments and mild arrhythmias) through different coronary arteries.

The paper is organized as follows. In Section II, we present a detailed description of each step involved in the proposed methodology and the parameter setup to ensure the automation of the method. In Section III, we present the validation of the method and a comparison with the state-of-the-art methods for image-based gating. Finally, Section IV presents the conclusions of this work.

II. METHODOLOGY

A. Integration of motion signals

Let us define the motion signal as a function $s(n)$ that measures the motion of the n-th image of the study. Then, $s(n)$ increases if the structures in the vessel change their distribution by translation, deformation or rotation with respect to the preceding/succeeding images. Besides, the image noise (speckle) produced by the micro-structures of the tissue [18] arises as a coherent pattern that varies through the different material composition in the vessel wall. For this reason, the noise variations that increment $s(n)$ are associated to movements or topological changes of the structures present in the images.

The signal $s(n)$ is chosen to be a linear combination of M image features, $s_i(n)$, $i = 0, \ldots, M - 1$, characterizing the motion in an image. Then, the function $s(n)$ is defined as

$$s(n) = \sum_{i=0}^{M-1} w_i \, s_i(n) \qquad (1)$$

where $w_i \in (0, 1)$ is the weight factor of the feature s_i and $\sum_{i=0}^{M-1} w_i = 1$.

In this work, we choose two features similar to those presented in [10] and [13], respectively. The first feature, $\hat{s}_0(n)$, is an inverse correlation between two consecutive images, that is

$$\hat{s}_0(n) = 1 - \frac{\sum_{i=1}^{H} \sum_{j=1}^{W} (u_n(i,j) - \mu_n)(u_{n+1}(i,j) - \mu_{n+1})}{\sigma_n \, \sigma_{n+1}}, \qquad (2)$$

where $u_n(i,j)$ is the intensity at the i-th row and j-th column, μ_n and σ_n are mean and standard deviation of the intensity for the n-th frame and H and W are the frame height and width. The choice of this feature is justified because the absence of movement is associated with two almost identical images, leading to a $s_0(n) \approx 0$. When the motion between the frames increases, the matching of structures decreases leading to smaller correlation. Although, the feature also increase in motionless scenarios such as topological changes (e.g. bifurcations) or the appearance of new structures (e.g. stents or calcium deposits). To improve the treatment of these scenarios, we use another feature for motion assessment, insensitive to differences between adjacent frames. This second feature, called $\hat{s}_1(n)$, measures the blurring in the image,

$$\hat{s}_1(n) = -\sum_{i=1}^{H} \sum_{j=1}^{W} |\nabla u_n(i,j)|, \qquad (3)$$

which exploits the fact that the transducer movement provokes a blurring effect at the borders of the structures.

To adequately combine the image features used to generate $s(n)$, we normalize their ranges as

$$s_i(n) = \frac{s_i^+(n)}{\sum_{n=1}^{N} s_i^+(n)} \qquad (4)$$

where

$$s_i^+(n) = \hat{s}_i(n) - \min_{1 \le n \le N} (\hat{s}_i(n)) \qquad (5)$$

and N is the number of images in the IVUS study. This last step ensures that all s_i are positive and of the same magnitude order. For the particular case of using two image features, the weighing factors can be reduced to only one parameter, α, defined as $w_0 = \alpha$ and $w_1 = 1 - \alpha$, thus

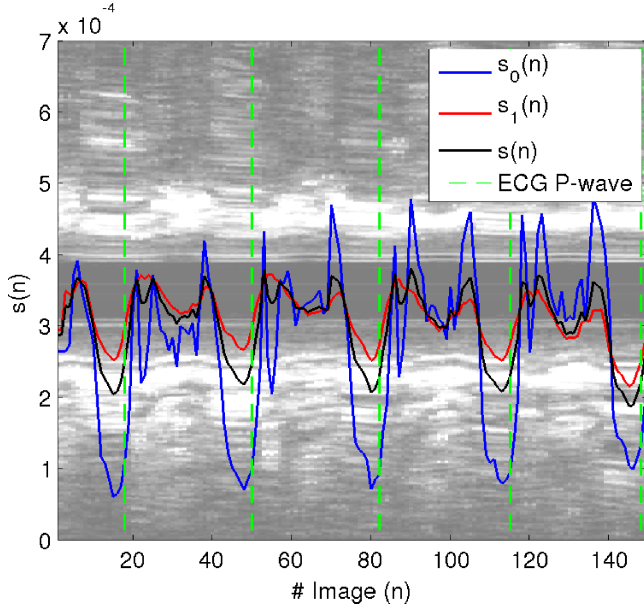$$s(n) = \alpha s_0(n) + (1 - \alpha)s_1(n). \qquad (6)$$

Fig. 1: Partial longitudinal view (first 150 frames) of an IVUS study presenting the motion signal $s(n)$ and the associated features, $s_0(n)$ and $s_1(n)$, using $\alpha = 0.25$. Also the P-wave occurrence from the synchronized ECG is marked.

The image features and the integrated signal are presented in Fig. 1 for a frame window in an in-vivo study. It is observed that several consecutive columns present a similar intensity pattern around the points of minima, which means the transducer is acquiring a set of almost identical frames. A pseudo-periodic pattern with equally separated minima is observed for $s(n)$. These minima are also present in the individual features and are equally displaced to the end diastolic phase (P-wave, marked with green dashed vertical lines) in each heartbeat. Therefore, we can infer a direct relation between these minima and a specific cardiac phase in the study.

B. Cardiac phase identification

Next goal is to detect the set of pseudo-periodic minima related to the specific cardiac phase previously described. As seen in Fig. 1, $s(n)$ presents many local minima in each heartbeat making non-trivial the automatic gating of this cardiac phase. But taking advantage of the $s(n)$ pseudo-periodicity, the frequency spectrum of $s(n)$ is analyzed and a low frequency version of $s(n)$ is created, eliminating spurious minima. To maintain the direct relation between the remaining minima and the physiological cardiac phases, the filtered low frequency signal must include a minimum amount of frequencies such that the original pulsation pattern is preserved. Otherwise, the lack of high order frequencies can lead to a poor representation of the pseudo-periodicity of the signal local minima.

The frequency spectrum of the signal, $\tilde{s}(k)$, is computed as the discrete Fourier transform of $s(n)$. In Fig. 2, the absolute value of the frequency spectrum $\tilde{s}(k)$ from an in-vivo IVUS study is presented. There, a local maximum frequency f_m in the range of physiologically valid heart frequencies is observed (0.75 Hz to 1.66 Hz or, equivalently, 45 BPM to 100 BPM).
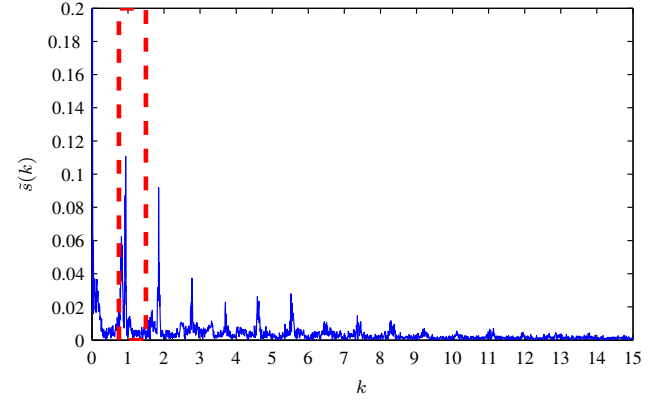

Fig. 2: Motion signal in the frequency domain. Red lines depict the range of physiologically valid heart frequencies.

As will be shown later f_m is a close approximation of the mean cardiac frequency along the study (see Section III-E). The use of f_m as cut frequency for a low-pass filter over $s(n)$ yields a filtered signal that preserves an approximate amount of heartbeats in the study. Therefore, the automatic detection of f_m is performed by extracting the maximum frequency component of $s(n)$ in the physiological range, i. e.,

$$f_m = \max_{k \in [0.75, 1.66]} (\tilde{s}(k)) \qquad (7)$$

where the physiological range is defined between 0.75 Hz and 1.66 Hz.

To consider the pseudo-periodicity of the signal we introduce a factor, δf_m, $\delta \in (0, 1)$, which models the deviation of the heartbeat frequency along the study. Then, the cut frequency for the low-pass filter is defined as

$$f_c = (1 + \delta) f_m. \qquad (8)$$

The low frequency signal, $s_{low}(n)$, is constructed as the convolution of $s(n)$ against a low-pass kernel $f(n)$, namely

$$s_{low}(n) = s(n) * f(n), \qquad (9)$$

where $*$ is the convolution operator. In turn, the low-pass kernel is defined as

$$f(n) = w(n) \cdot h(n), \qquad (10)$$

where $w(n)$ is the equivalent of a rectangular unitary window for the frequencies $k \in [0, f_c]$ and $h(n)$ is a Hamming window of N points. The approximations involved with the Fourier discrete transform are avoided by applying this kernel in the time domain. Thus, the expression of $f(n)$ is given by

$$f(n) = \left[\frac{f_c}{f_{max}} \text{sinc}\left(\frac{f_c n}{f_{max}} \right) \right] \left[\tau - \nu \cos\left(2\pi \frac{n}{N} \right) \right], \quad (11)$$

where f_{max} if the maximum frequency in the study calculated as half of the transducer frame rate. In the equiripple sense, optimal values for the Hamming window are chosen as $\tau = \frac{25}{46}$ and $\nu = \frac{21}{46}$ (see [19], [20]).

The resulting signal $s_{low}(n)$ presents approximately one minimum for each heartbeat, which provides a first approximation for the local minima positions $p(i)$, at the i-th heartbeat.
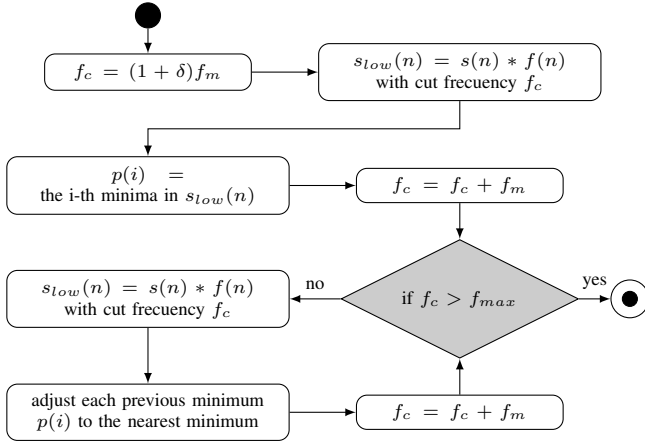
Fig. 3: Activity diagram detailing the iterative adjustment of $p(i)$ from the initial signal $s_{low}(n)$ to $s(n)$.

Using this initialization, the iterative scheme presented in Fig. 3 is applied. At each step, all frequencies up to the next harmonic component are incorporated in the definition of $s_{low}(n)$ and $p(i)$ is adjusted to the nearest local minimum. Note that, the adjusted value of $p(i)$ is not necessarily the i-th minimum of $s_{low}(n)$ because addition of higher frequencies may induce the apparition of additional minima. This process is repeated until $s_{low}(n)$ incorporates all harmonic components of f_m, obtaining the adjusted minimum for each heartbeat.

In Fig. 4, the evolution of $s_{low}(n)$ through the incorporation of frequencies is observed along the f_c axis. It can be seen that the initialization of the minima in $s_{low}(n)$ can be displaced from the pseudo-periodic minima of $s(n)$ due to the absence of high frequency contributions. As we incorporate harmonic components of $s(n)$ progressively, the minima is adjusted smoothly (red points path in the f_c axial direction) to the associated minima position at the signal $s(n)$. This increases the precision of the $p(i)$ locations, for the cardiac phase detection.

C. Decomposition in cardiac phases

The identification of the images corresponding to the detected cardiac phase, i. e. the ones acquired at the $p(i)$ instants, allows the decomposition of the study in sets of images associated to each heartbeat. This is done by grouping the images between $p(i)$ and $p(i+1)$ as the set of images acquired in the i-th heartbeat. In this manner, the number of sets found, is equivalent to the number of heartbeats identified in the IVUS study.

Over these new sets of images, we define $\mathrm{HB}(i,j)$ as the index (frame number) in the original IVUS study of the j-th image corresponding to the i-th heartbeat in the study. In this indexation $\mathrm{HB}(i,1)$ represents the images at the first identified cardiac phase (i.e., the frames acquired at $p(i)$).

Since the heart frequency changes along the study, the heartbeats are sampled with a variable amount of frames. This variability in the heartbeat affects mainly the time of the diastole (more specifically the T-P interval), i. e. the heart relaxes during a major or minor period of time. Although, the cardiac

waves duration associated with the cardiac phases show almost no change at all. As consequence, longer heartbeats present more cardiac phases than a short heartbeat.

Then, P cardiac phases for the i-th heartbeat are identified as the first P frames. The value of P is chosen as the amount of frames of the shortest heartbeat in the study. The reason behind this choice was to preserve axial spacing as homogeneous as possible between images from different cardiac phases. This guarantees that each phase is represented by the same amount of information.

Finally, the set of images $U^k(i)$ corresponding to the k-th cardiac phase is defined as

$$U^k(i) = I(\mathrm{HB}(i,k)), \qquad i = 1, \ldots, B, \ k = 1, \ldots, P \quad (12)$$

where $I(n)$ is the n-th image of the IVUS study and B is the quantity of heartbeats along the study.

D. Parameter setup

An analysis for the parameters α and δ (Eq. (6) and (8), respectively) is performed to ensure an appropriate and automatic execution of the method.

1) Parameter α: IVUS studies present small variations in the cardiac period during acquisition for patients without severe cardiac arrhythmia. For this reason, the criteria used to choose the optimal α is to reduce the heartbeat period variability detected with the gating method (see Section III-H for associated implications). This is simply done by minimizing the standard deviation of the set of values $p(i+1) - p(i)$ for $i = 1, \ldots, B - 1$.

In this manner, an optimization problem is solved to determine the optimal α parameter that efficiently combines the features s_0 and s_1 for an specific IVUS study. This minimization process is performed by testing a large number of candidates, say $\alpha_c, c \in C$ being C the set of candidates, and then picking the best fitting one for the aforementioned criteria. Combining s_0 and s_1 with a particular α and computing the adjusted minima $p(i)$ are computationally cheap tasks, then we can apply a brute force minimization scheme with low computational cost.

To formalize this, let us define $t_{\mathrm{HB}}^{\alpha_c}(i) = p(i+1) - p(i)$ as the period of the i-th heartbeat from the signal $s(n)$ calculated with α_c and $\sigma_t^{\alpha_c}$ as the standard deviation of the periods $t_{\mathrm{HB}}^{\alpha_c}(i)$ for the entire study, then the optimal α is obtained as

$$\alpha = \arg \min_{\alpha_c \in C} \sigma_t^{\alpha_c}. \quad (13)$$

To determine an appropriate quantity of α_c values used in the calculus of α, we evaluate the variation of the minimum $\sigma_t^{\alpha_c}$ from Eq. (13) for different sizes of C. We define C as a set of equally spaced candidates $C = \{\alpha_c^i; \alpha_c^i = i/A, \ i = 0, \ldots, A\}$ where A is the quantity of α_c candidates to be tested in Eq. (13). For the set of studies available (61 studies), a suitable size of C was given by $A = 10^3$, for which the error of estimating $\sigma_t^{\alpha_c}$ was smaller than 10^{-3} seconds.

The α value from Eq. (13) varies among studies due to their vessel topology and intensity of sensor motion. As commented before, s_0 does not accurately represent motion for studies
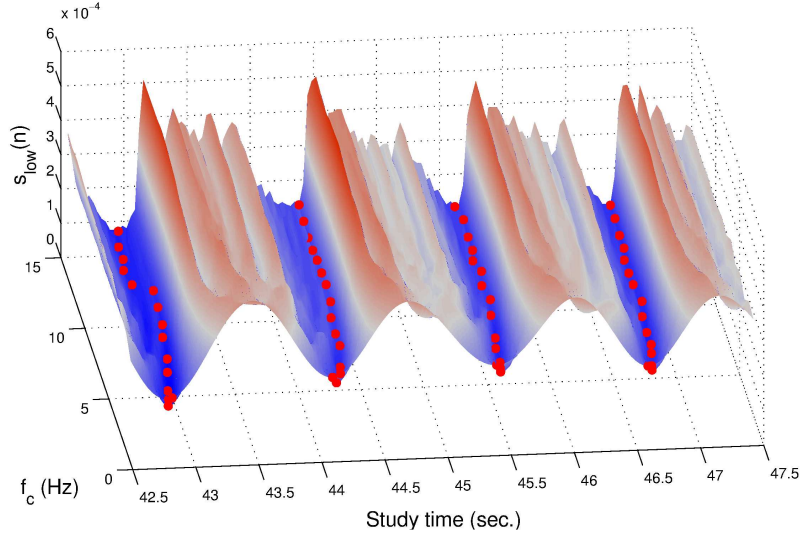
Fig. 4: Evolution of the iterative scheme for adjusting the minima position. The axis f_c corresponds to the cut frequency of the low-pass filter and, at each fixed value of this axis, the $s_{low}(n)$ associated signal is presented. The red dots mark the position of the adjusted minima, $p(i)$, corresponding to the identified cardiac phase.

with numerous topological changes (bifurcations, dissections, etc.) then a lower α is expected for these cases. On the other hand, studies with poor blurring (usually associated with low sensor motion during acquisition) will produce a unreliable s_1, increasing the value of α.

This setup is straightforward generalized for the integration of K motion signals by performing the same optimization scheme over the K dimensional space defined by the weight factors $\mathbf{w} = w_1, w_2, \ldots, w_K$ (see (1)). The optimal weights factors of the features are obtained as

$$\mathbf{w} = \arg \min_{\mathbf{w} \in C_{\mathbf{w}}} \sigma_t^{\mathbf{w}} \qquad (14)$$

where $C_{\mathbf{w}} = C_{w_1} \times C_{w_2} \times \ldots \times C_{w_K}$ and C_{w_i} is the set of candidates for the weight factor w_i.

2) Parameter δ: The range $\delta \in (0, 1)$ guarantees no harmonic contributions in each low-pass filter iteration. This ensures that the signal $s(n)$ contains only one minima at each heartbeat. Meanwhile, the variability in the heartbeat frequency can mislead the detection of the heartbeats for values of δ near the range limits.

For the lower limit, when δ is close to 0, the heartbeats with frequency above f_m are not recovered in $s_{low}(n)$. For the superior limit, when δ is close to 1, we are recovering in $s_{low}(n)$ a harmonic contribution for the heartbeats with frequency below f_m. As result, we would be generating two local minima for the heartbeats with duration above the mean heartbeat duration. Both cases are unacceptable because they introduce inaccuracies to the initialization of our minima adjustment scheme (Fig. 3).

For these reasons, intermediate values render better results. Concretely, a good agreement was empirically obtained for $\delta = 0.4$, which presented no omission nor addition of minima in comparison with the data retrieved from the ECG signal. Theoretically this value is also valid given that variability in

the heartbeat frequency above 40% of the mean is not usually seen in patients without severe cardiac arrhythmia.

III. RESULTS

The proposed method was validated using IVUS images with a synchronized ECG signal. A manual offline ECG gating was chosen as ground truth for comparison, where a specialist determine the frames at the R-wave peak by inspection of the ECG signal. Moreover, other state-of-the-art methods described in the literature were implemented for comparison, namely Absolute Intensity Difference (AID) [4], Correlation Dissimilarity Matrix (CDM) [10] and Motion Blur (MB) [13]. It is worth noting that the image feature combined by our method are the presented in CDM and MB. A direct comparison between the three methods is useful to assess the improvement introduced by our proposal.

A. Acquisition of in-vivo IVUS studies

The IVUS studies were acquired with the Atlantis$^{\text{TM}}$SR Pro Imaging Catheter 40 MHz synchronized with an ECG signal and connected to an iLab$^{\text{TM}}$ Ultrasound Imaging System (both by Boston Scientific Corporation, Natick, MA, USA), at the Heart Institute (InCor), University of São Paulo Medical School and Sírio-Libanês Hospital, São Paulo, Brazil. The acquisition frame rate was of 30 FPS performing for each frame 256 radial scans with 256 intensity measurements. The generated frames of 512×512 pixels in cartesian coordinates present a resolution of $17.5\,\mu\text{m} \times 17.5\,\mu\text{m}$ per pixel.

The procedure was performed during a diagnostic or therapeutic percutaneous coronary procedure. Vessels were imaged during automated pullback at 0.5 mm/s, but additional manual runs, not used in the subsequent analysis, were performed. Overall, multiple runs where performed on 21 patients leading to 61 IVUS studies with synchronized ECG signal. The IVUS sequence length reported in these studies comprises

2974.8 ± 1133.8 frames (mean ± SD). Images from different coronary arteries (Left Anterior Descending - LAD, 31 studies; Right Coronary Artery - RCA, 8 studies; Left Circumflex Artery - LCx, 12 studies; and Obtuse Marginals and Diagonals, 10 studies) at different mean cardiac frequencies (from 65 BPM to almost 105 BPM) including cases with severe stenosis, stent deployment and mild arrhythmia (presence of $\leq$ 5 extrasystole in 9 studies) were analyzed.

After the procedure, a manual offline ECG gating was performed for each study. Specifically, a specialist marks, as shown in Figure 5, the elapsed time at each R-wave peak over the ECG signal of each study. Using that information, the period of each cardiac cycle in the studies is calculated. As the IVUS study is synchronized with the ECG signal, the R-wave peak frames are identified and the gating of this phase is used as ground truth. As the time between the beginning P-wave and the R-wave peak rarely varies, it is reasonable to infer the period between the steady phase as the period between the R-wave peaks.

Manual R-wave peak segmentation reliability was estimated by calculating intra- and inter-observer variability in terms of the Bland-Altman limits of agreement (LA) and the coefficient of variability ($\%CV$). Thus, 3 specialists segment 3 times 5 studies (with 77, 112, 130, 130 and 165 R-wave peaks giving $N = 614$ samples). For intra-observer variability, we compare among the repeated segmentations of a fixed specialist to observer the degree of variation. The results are presented in Table I where it is seen that variations within each specialist are less than 1 frame (maximum variation of 0.3634 frames for the specialist 3 between segmentations 1 and 3), showing negligible variability in the segmentation process. Inter-observer variability was addressed by estimating the mean observation, $\overline{O}_i$, corresponding to the i-th specialist. The values of $\overline{O}_i$ are simply the mean values of each R-wave peak time from the 3 repeated segmentations of the i-th specialist. This step attenuates the intra-observer variability in order to deliver a more reliable inter-observer analysis. The results presented in Table II suggest even lower variability than intra-observer analysis (worst case present a discrepancy of 0.184 frames between specialist 2 and 3), indicating a high level of agreement between specialists about this ground truth.

B. Features correlation

The main purpose of constructing a combined signal from two image features is to increase the robustness of the heart motion estimation. Thus, we seek for features uncorrelated that at the same time present a close motion pattern associated with the heartbeat. As the features present a low correlation, their combination presents minimal redundancy, implying that the motion is characterized in different manners by each feature.

In that manner, we analyze the correlation between the features s_0 and s_1, by computing the Pearson's linear correlation between them. As result, we obtain a mean correlation of -0.164 ± 0.266 (mean ± SD), presenting scarce redundancy of information. Meanwhile, both features present a similar motion frequency, characterized by f_m from (7), showing a shallow absolute difference of 0.0146 ± 0.0263 heartbeats per
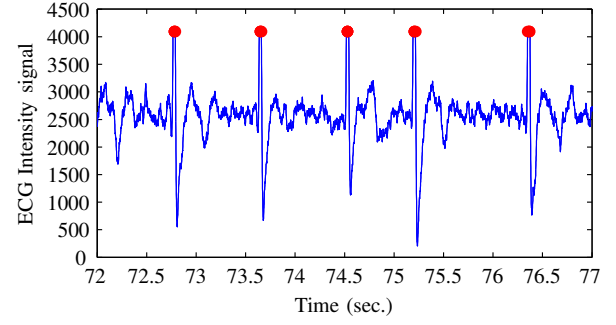

Fig. 5: ECG signal depicting the specialist red marks at R-wave peak instants. The marks are then associated to the frames acquired at these instants according with the IVUS DICOM header. This example shows 5 seconds of the ECG signal synchronously acquired during the IVUS pullback by the iLab$^{\text{TM}}$ Ultrasound Imaging System.

second (mean ± SD) along the studies. The resemblance in f_m allow us to infer that both feature reproduce a closer pseudo-periodic pattern associated with the transducer motion.

C. Error measurements

The proposed image-based gating method was assessed using two quality measures. For the sake of simplicity, we introduce some definitions first. Let us generalize the definition of $p(i)$ as the time at which a particular cardiac event occurs at the i-th heartbeat of the study, e. g., the R-wave peak in the ECG signal ($p^{\text{ECG}}(i)$) or the minima in an image-based method ($p^{\text{IB}}(i)$). From $p(i)$ then we can derive $t_{\text{HB}}(i)$ and $p_m(i)$, the heartbeat period and the middle time instant of the i-th heartbeat of the study, as

$$t_{\text{HB}}(i) = p(i+1) - p(i)$$
$$p_m(i) = \frac{t_{\text{HB}}(i)}{2} + p(i).$$

The **mean error per heartbeat**, ε_{HBP}, measures the mean period difference between the image-based and the offline ECG gating method. For each heartbeat its period, obtained from the image-based gating, is compared with the nearest period from the ECG gating as

$$\varepsilon_{\text{HBP}} = \frac{\sum_{i=1}^{M} \left| t_{\text{HB}}^{\text{IB}}(i) - t_{\text{HB}}^{\text{ECG}}\left(\min_j \left(\left| p_m^{\text{IB}}(i) - p_m^{\text{ECG}}(j) \right| \right) \right) \right|}{M}$$

(15)

where M is the quantity of cardiac events detected by the image-gating method and $(\cdot)^{\text{IB}}$ and $(\cdot)^{\text{ECG}}$ are quantities associated with the image-based gating method and the offline ECG gating method, respectively. Using this error measurement, the omission or erroneous detection of the $p(i)$ event does not affect the error estimation in the next cardiac cycles. Notice that the quantity of heartbeats in a study according to the gating method is equal to $M - 1$.

The **phase detection error**, ε_{PD}, measures the difference between the R-wave peak detected by the image-based and the ECG gating methods. As previously mentioned, the time

	S_1 vs S_2		S_1 vs S_3		S_2 vs S_3	
	LA (in frames)	$\%CV$	LA (in frames)	$\%CV$	LA (in frames)	$\%CV$
O_1	-0.0130 ± 0.2351	0.012	-0.0098 ± 0.2553	0.014	0.0033 ± 0.2285	0.012
O_2	-0.0081 ± 0.2647	0.014	0.0016 ± 0.2457	0.013	0.0098 ± 0.2210	0.012
O_3	0.0033 ± 0.3521	0.019	0.0163 ± 0.3471	0.018	0.0130 ± 0.3425	0.018

TABLE I: Intra-observer variability from 3 segmentations (S_1, S_2 and S_3) per specialist (O_1, O_2 and O_3). Bland-Altman limits of agreement (LA) and coefficient of variations ($\%CV$) are presented for each comparison.

	LA	$\%CV$
$\overline{O_1}$ vs $\overline{O_2}$	-0.0141 ± 0.1196 frames	0.006
$\overline{O_1}$ vs $\overline{O_3}$	-0.0038 ± 0.1729 frames	0.009
$\overline{O_2}$ vs $\overline{O_3}$	0.0103 ± 0.1737 frames	0.009

TABLE II: Inter-observer variability from mean values of the 3 intra-observer segmentations. Bland-Altman limits of agreement (LA) and coefficient of variations ($\%CV$) are presented for each comparison.

elapsed between the P-wave and the R-wave peak rarely varies (independently of the heartbeat frequency variations), then we can identify the R-wave peak frames in the image-based gating by displacing all P-wave frames with the same offset. As we want to retrieve the most similar phase to the R-wave peak, we calculate this offset as the mean distance between $p^{\text{IB}}(i)$ events to the p^{ECG}, given by

$$
\mu_{\text{PD}} = \frac{\sum_{i=1}^{M} \left[p^{\text{ECG}} \left(\min_{j} \left(|p_m^{\text{IB}}(i) - p_m^{\text{ECG}}(j)| \right) \right) - p^{\text{IB}}(i) \right]}{M}.
\tag{16}
$$

Thus, we calculate the error at each heartbeat as the distance between the p^{ECG} instant and the p^{IB} displaced by μ_{PD}, namely

$$
\varepsilon_{\text{PD}}(i) = p^{\text{IB}}(i) + \mu_{\text{PD}} - p^{\text{ECG}} \left(\min_{j} \left(|p_m^{\text{IB}}(i) - p_m^{\text{ECG}}(j)| \right) \right),
\tag{17}
$$

with $i = 1, \ldots, M$.

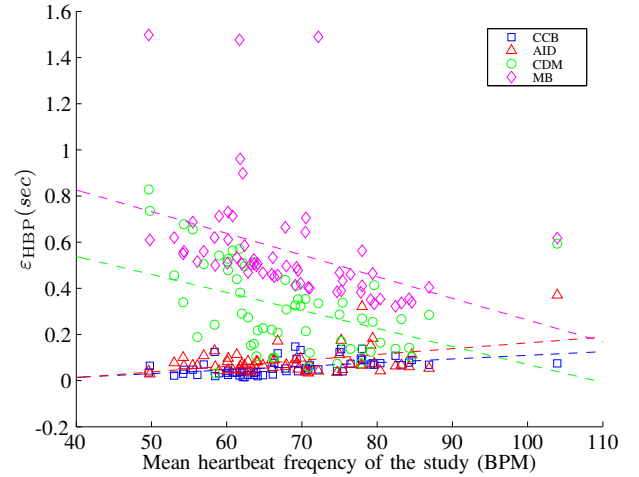Fig. 6: Error ε_{HBP} at each study for the different gating methods. The dashed lines represents a linear fitting (via linear least-squares) that describes the error behaviour for each method.

D. Method performance

The performance of the CCB method was evaluated through comparisons with the following methods: Absolute Intensity Difference (AID), Correlation Dissimilarity Matrix (CMB) and Motion Blurring (MB). The comparison of our method against [10] and [13] shows the improvement obtained by the integration of both motion signals and, also, from the proposed cardiac phase identification strategy.

In the first comparison, the capability of the different methods for predicting the cardiac cycles periods is compared. The heartbeat periods estimated via the ECG offline method were used as ground truth. In Fig. 6 the error ε_{HBP} for the four methods is shown. The CCB method presents the best behaviour as indicated by the linear fitting in the same figure, followed by the AID method. The variability of the error is also smaller for the CCB method and increases of the cardiac frequency barely increment its error.

An additional comparison between the image-based methods and the ECG offline gating method is featured in Fig. 7. In this case, we present the heartbeat period estimation for each heartbeat in every study (61 studies). The Bland-Altman coefficient of reproducibility (RPC= $1.96 \times$ SD) is the smallest

for CCB, RPC(%) = 0.23 sec. (26%), followed by AID with RPC(%) = 0.36 sec. (41%). This implies that the CCB method is the closest one to the manual offline ECG gating. The proposed method also presents a more robust estimation of the heartbeat period evidenced by the reduced dispersion and range of samples in the y-axis (see Fig. 7).

Using the acquisition time of frames at R-wave peak according to the manual offline ECG gating, we evaluate the performance of the methods. Since the R-wave peak is the only cardiac phase that we can extract precisely from the ECG, this is the only indicator where the success in recognizing a specific cardiac phase can be measured. For this reason, the ε_{PD} error is a trustful indicator of success when using p^{ECG} as the R-wave peaks. As the mean of this error is zero by construction, we are interested in its standard deviation along each study, which shows differences between the gated phase and the ground truth. The value of this indicator is presented in Fig. 8 where the mean and maximum standard deviation for the 61 studies using each of the 4 methods are shown. The CCB method presents the most accurate results, with mean SD of ε_{PD} being 0.165, 0.251, 0.282 and 0.475 for the CCB,
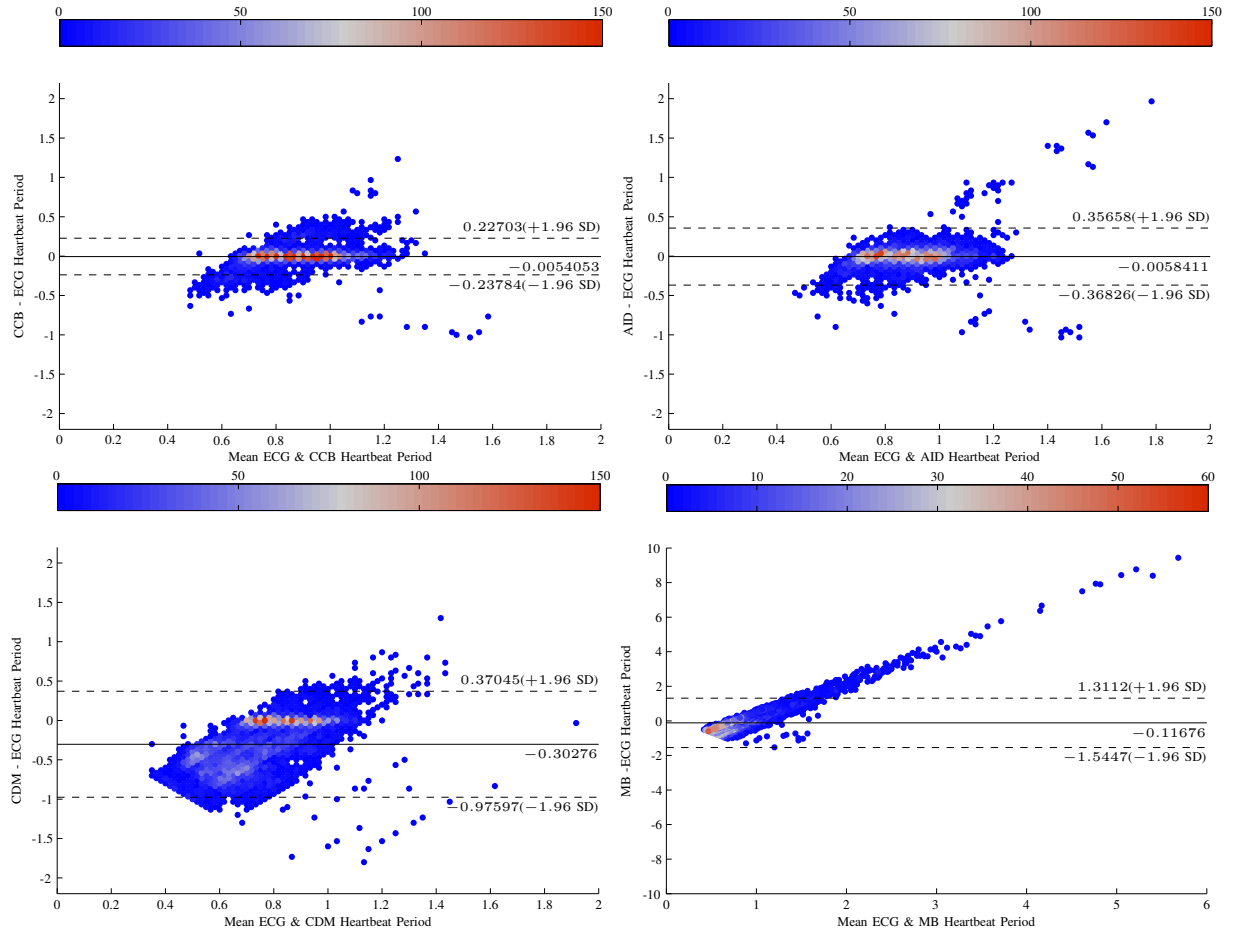
Fig. 7: Bland-Altman plots comparing the heartbeat periods measured by the offline ECG method (assumed as ground truth) and : (a) the CCB method presenting RPC(%)= 0.23 sec (26%); (b) the AID method presenting RPC(%)= 0.36 sec (41%); (c) the CDM method presenting RPC(%)= 0.67 sec (90%); (d) the MB method presenting RPC(%)= 1.4 sec (170%). Each sample represents one heartbeat period in one of the studies. The color indicates the amount of samples overlapped in the same position of the diagram, horizontal solid line stands for the mean difference and dashed line depict the limits of agreement (1.96× standard deviation of the differences). Plots (a)-(d) contain respectively 6802, 6614, 10077 and 7651 samples corresponding to 61 studies.

AID, CDM and MB methods, respectively.

From the analysis of these results, it is seen that MB presents outliers exceeding 0.8 seconds (see Fig. 6) caused by the omission of several frames associated with the steadiest phase. In these studies the transducer motion is too low to produce the blurring effect, at least not along the full study. Then, the motion signal poorly represents the cardiac pulsatility and does not present the characteristic quase-periodic pattern (the frames extracted do not represent any specific phase, see Fig. 8). CCB circumvents this issue by the adjustment of α performed in Eq. (13). As s_1 shows high variation of heartbeat periods, α is adjusted to values closer to 1 giving major weight to s_0 data (which resembles the signal used in AID).

In another analysis, we compare the number of heartbeats estimated by each method against the ground truth. Here, it is evident that the methods using band pass filter around the mean cardiac frequency (i.e. CCB and AID) delivered better results (see Table III). This is given by the low heartbeat frequency variation within a study. As extra systoles may
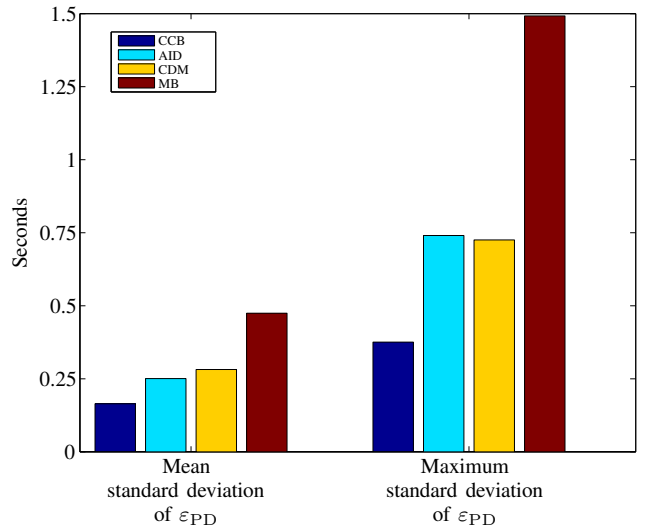

Fig. 8: Mean and maximum standard deviation of the error measure ε_{PD} for each of the gating methods.

Id	CCB	AID	CDM	MB
Mean error	1.492	4.246	52.984	24.623
SD error	0.977	3.567	48.028	19.068
Maximum error	6	22	219	80

TABLE III: Number of heartbeats (frames in the longitudinal view) detected by each gating method. The error in the i-*th* study is calculated as $|B^{\mathrm{ECG}} - B^{\mathrm{IB}}|$ where B^{ECG} and B^{IB} are the heartbeats estimated in the ground truth and the image based method respectively.

occur in a study from time to time, the cardiac frequency remains almost invariant and the use of this information is fundamental to provide robustness to the method. Methods like CDM and MB do not assume low variation of the cardiac frequency, making them potentially capable of detecting any kind of cardiac variations. Although, these methods would also be capable of detecting extremely shorts heartbeats (most of the times physiologically meaningless) which would yield an incoherent phase gating. Particularly, CCB method presents a better performance compared to the other methods (even against AID) diminishing the number of frames omitted or oversampled for the extracted cardiac phase. For the CCB, less than 6 beats per study are missed or overestimated presenting a mean error of 1.492 ± 0.977 heartbeats (mean $\pm$ SD) along all the studies. As consequence, the proposed method presents a larger proportion of phase coherent data extracted from the study for a specific cardiac phase.

From the different comparisons, AID and CCB reported the closer heartbeat period detection mainly because the use of a band filter around the mean cardiac frequency of the study. Their motion signals present low heartbeat period variations (as higher frequencies were removed) as is physiologically expected. Thus, an accurate prediction of mean heartbeat periods and number of heartbeats present in the study is obtained. Although, AID is not phase consistent, i.e. the identified frames are not necessarily associated with the same cardiac phase, as can be shown in Fig. 8. In turn, CCB underpins this issue by combining the motion signal s_0 (associated with frames correlation) with another uncorrelated motion signal (associated with blurring). The resulting signal intensity decreases at the steadiest phase frames while increases at the remaining phases frames. Then, when minima are adjusted by the iterative harmonic scheme, we obtain a more accurate steadiest phase identification.

E. Mean cardiac frequency estimation

Using the ground truth, we compute the mean cardiac frequency, f^{ECG}, as the quantity of heartbeats detected over the study time duration. Then, we compare f^{ECG} against f_m calculated using Eq. (7) in terms of their absolute difference, i. e., $\varepsilon_{\mathrm{HF}} = |f^{\mathrm{ECG}} - f_m|$. The comparison shows an error of 1.109 ± 0.861 BPM (mean $\pm$ SD), and always minor than 4.126 BPM. This allows estimating the mean cardiac frequency of the patient with reasonable accuracy, only by using the IVUS image data.

F. Gating comparison

As a qualitative comparison, the corresponding longitudinal views after the gating process with the different methods for a particular IVUS study are shown in Fig. 9. The endothelial layer gated by the offline ECG method clearly resembles the result of the CCB method more than those obtained with other methods. This comparison is accentuated when looking at the differences between our ground truth and the different methods (see Fig. 9, right column). This can be seen at the bifurcation presented in the middle section of the sequence, where delay or anticipation of the branch origin occurs for other methods (CDM, AID and BM). Moreover, a substantial reduction of *saw tooth artifact* is remarkable for the results given by CCB and AID methods.

The distribution of the differences between the image based and the offline gating method is not homogeneous. As shown in Fig. 10 the maximum differences are located at the middle part of the vessel where the bifurcation is located. This encourages the use of features that correctly measure the motion while topological changes occur. In fact, small differences are seen for the CCB method, where blurring information reduces motion misidentification.

G. Computational Cost

The method was implemented partially in MATLAB and C++ languages. The signal s_i calculation is performed in C++ parallelized at frame level with OpenMP. Alpha estimation (see Eq. (13)) and the iterative filtering scheme are performed in MATLAB using *parfor* parallelization for alpha estimation.

For the method execution, we used a workstation with an Intel Xeon CPU E5-2620 at 2.00 GHz processor and Kingston 99U5471-031.A00LF at 1333 MHz (latency of 27 ns) RAM memory over Ubuntu 14.04.1 LTS. The method execution process was parallelized into 12 threads for all the measurements reported in this section. As performance measurement, we use the wall clock time because we are interested in showing that the execution time is reasonable for clinical use. To diminish the operative system time variations during the method execution, we run 5 times each study processing, and store only the mean wall clock time from these executions.

The results show that the execution time is 20.63 ± 8.11 seconds (see Fig. 11) which in comparison to the acquisition time of the study (99.16 ± 37.79) represents 20%. This overhead is found to be suitable for medical practice since it allows to perform image gating during the diagnostic or therapeutic procedure. In a closer analysis, it is seen that the time consuming tasks are the α estimation and signal computation (see Fig. 11 and 12). Both tasks could be fully parallelized with a maximum of A and N threads, respectively, where A is the number of alpha candidates to be tested in Eq. (13) and N is the quantity of frames in the IVUS study. As reported in Section II-D1 and III-A, $A = 1000$ and $N = 2974.8 \pm 1133.8$ frames which allows a theoretical speed up of the methods until two order of magnitude from the reported results. Finally, almost all the estimation time for the value of α is spent in the iterative adjustment of $p(i)$
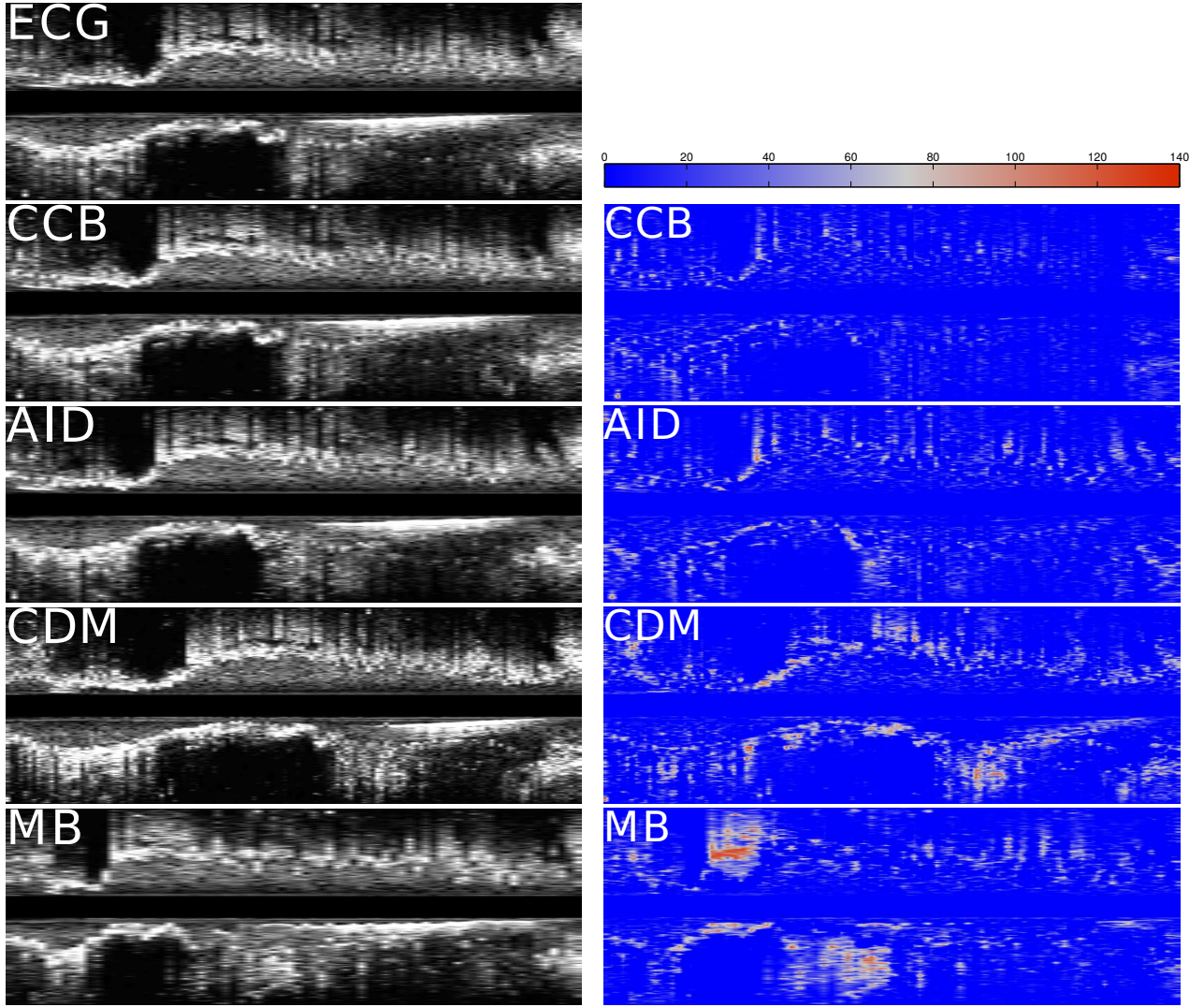
Fig. 9: Longitudinal views of an IVUS study processed with the different gating methods: (left column) standard longitudinal view; (right column) absolute difference versus the ECG offline method.

(see Fig. 12). This task is was implemented in MATLAB and parallelized using *parfor*. Clearly, its performance can be improved by reimplementing the task in C++ with OpenMP parallelization.

H. Limitations

Known limitations of this method, as well as for other methods using a low/band-pass filters at the spectral filtering of a motion signal, are related to the treatment of IVUS studies in patients with large heart rate variability, such as cardiac dysrhythmia, or at locations with no vessel movement at all, such as infarcted areas of the heart.

IV. CONCLUSIONS

A novel method to improve the IVUS gating by combining different image motion features has been presented. Particularly, the implementation, called Combined Correlation and Blurring, has shown to outperform other methods that use the same image features separately. The proposed method is capable of identifying cardiac phases, heartbeats and mean cardiac frequency along the studies in an accurate and robust manner for a wide range of situations (severe stenoses, stents, different coronary vessels and studies from 65 to almost 105 BPM). This has been verified through direct comparison with the cardiac phase associated to the R-wave peak, retrieved from a manual offline ECG gating with scarce intra-inter observer variability.

In terms of heartbeat detection and cardiac period estimation, the CCB method outperforms other compared methods. The cardiac phase detection performed by the CCB method presents the smallest error between the image-based gating methods, rendering the most accurate gating for IVUS study. From the comparisons carried out in this work, it presents the lowest frame omission and/or oversampling at each heartbeat, as direct consequence of the correct identification of the heartbeats along the study.

In contrast to the time consuming manual offline ECG gating, it is worthwhile to highlight that our method is fully
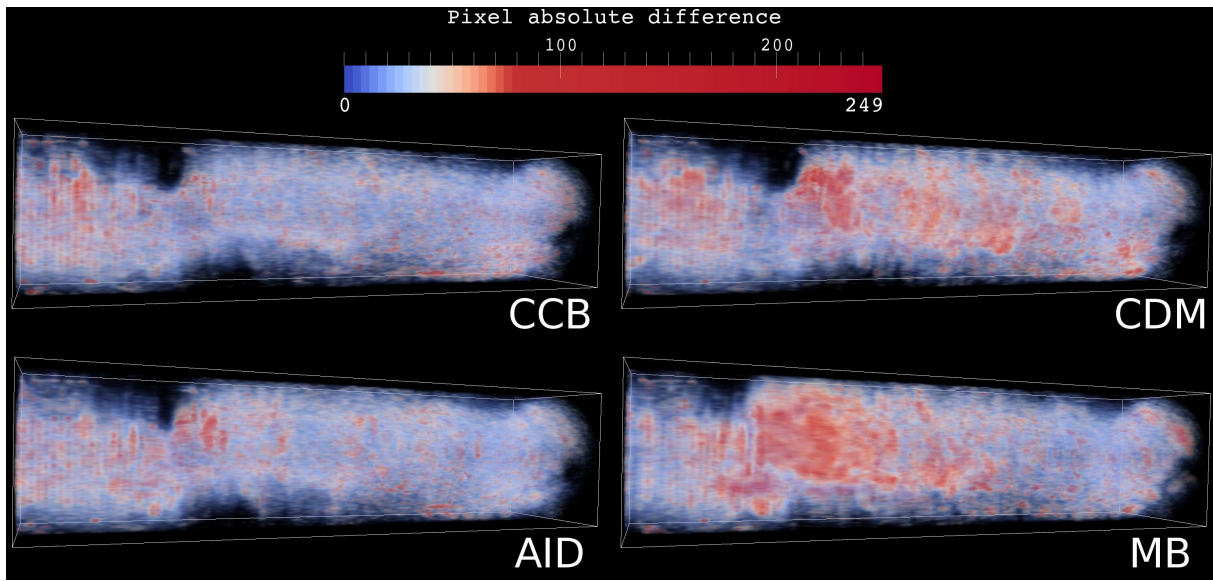
Fig. 10: Volume rendering corresponding to the absolute difference pixel to pixel of the volumes gated by the image based gating method and the manual offline ECG gating. The study visualized is the same as in Fig. 9.
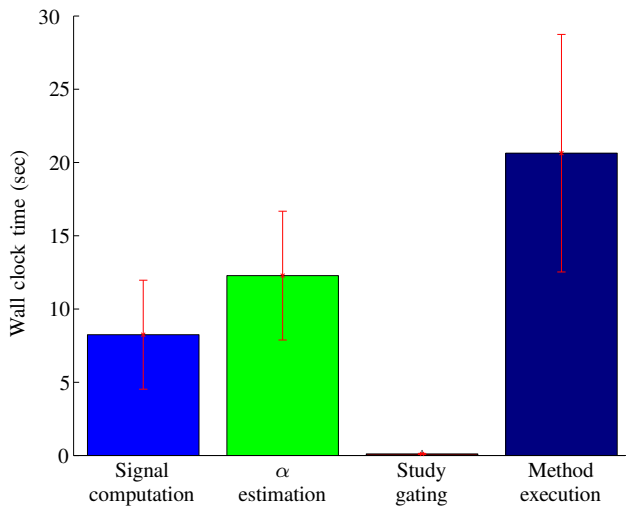

Fig. 11: Mean processing time of the 61 IVUS studies showing the time for: the signal computation (Eq. (2) and (3)), α estimation (Eq. (13)), study gating (Section II-B and II-C) and total method execution time.

Fig. 12: Percentage consumed by each method subtask during the execution. The task α estimation presented in Fig. 11 here is subdivided in the tasks: iterative adjustment of $p(i)$ and other tasks for α estimation.

automatic, independent from other studies or equipment and it is applicable to pre-existing IVUS studies. Also, the computational overhead of this method to the IVUS acquisition time is a 20%, allowing its use for medical practice during the diagnostic or therapeutic percutaneous coronary procedure. All these aspects permit the direct application of the CCB method as a pre-processing stage for filtering, segmentation or reconstruction methods, which would be greatly benefited from the increase of accuracy and time consistency of the so-extracted cardiac phases from the IVUS study.
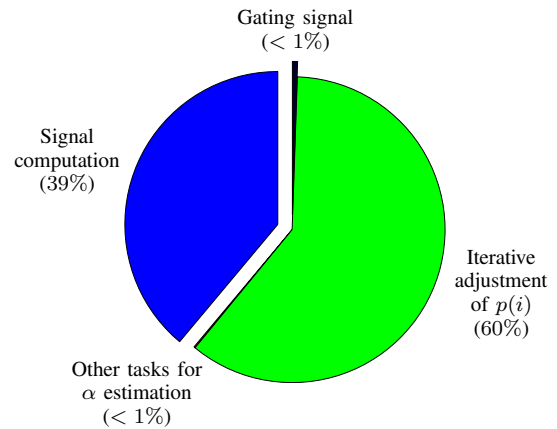
V. ACKNOWLEDGEMENTS

Conflict of Interest: The authors declare that they have no conflict of interest.

Ethical approval: For this type of study formal consent is not required.

REFERENCES

[1] Y. Honda and P. J. Fitzgerald, "Frontiers in intravascular imaging technologies," *Circulation*, vol. 117, no. 15, pp. 2024–2037, 2008.

[2] N. Bruining et al., "Ecg-gated versus nongated three-dimensional intracoronary ultrasound analysis: implications for volumetric measurements," *Catheter Cardio. Diag.*, vol. 43, no. 3, pp. 254–260, 1998.

[3] A. Arbab-Zadeh et al., "Axial movement of the intravascular ultrasound probe during the cardiac cycle: implications for three-dimensional reconstruction and measurements of coronary dimensions," *Am. Heart J.*, vol. 138, no. 5, pp. 865–872, 1999.

[4] H. Zhu, "Retrieval of cardiac phase from ivus sequences," in *Medical Imaging 2003*. International Society for Optics and Photonics, 2003, pp. 135–146.

[5] S. A. De Winter et al., "A novel retrospective gating method for intracoronary ultrasound images based on image properties," in *Computers in Cardiology, 2003*. IEEE, 2003, pp. 13–16.

[6] S. K. Nadkarni et al., "Image-based cardiac gating for three-dimensional intravascular ultrasound imaging," *Ultrasound Med. Biol.*, vol. 31, no. 1, pp. 53–63, 2005.

[7] J. Barajas et al., "Cardiac phase extraction in ivus sequences using 1-d gabor filters." in *Engineering in Medicine and Biology Society, 29th Annual International Conference of the IEEE*. IEEE, 2007, pp. 343–346.

[8] C. Gatta et al., "Robust image-based ivus pullbacks gating," in *Medical Image Computing and Computer-Assisted Intervention - MICCAI 2008*, vol. 11, no. 2. Springer Berlin Heidelberg, 2008, pp. 518–525.

[9] S. M. O'Malley et al., "Image-based frame gating of ivus pullbacks: A surrogate for ecg," in *Acoustics, Speech and Signal Processing, 2007. ICASSP 2007. IEEE International Conference on*, vol. 1, 2007, pp. I–433–I–436.

[10] S. M. O'Malley et al., "Image-based gating of intravascular ultrasound pullback sequences," *Information Technology in Biomedicine, IEEE Transactions on*, vol. 12, no. 3, pp. 299–306, 2008.

[11] A. Hernandez et al., "Image-based ecg sampling of ivus sequences," in *Ultrasonics Symposium, 2008. IUS 2008. IEEE*, 2008, pp. 1330–1333.

[12] M. S. Matsumoto et al., "Cardiac phase detection in intravascular ultrasound images," in *Medical Imaging 2008: Ultrasonic Imaging and Signal Processing*, vol. 6920, 2008, pp. 69 200D–69 200D–9.

[13] C. Gatta et al., "Real-time gating of ivus sequences based on motion blur analysis: method and quantitative validation," in *Medical Image Computing and Computer-Assisted Intervention - MICCAI 2010*, vol. 13, no. 2. Springer Berlin Heidelberg, 2010, pp. 59–67.

[14] G. G. Isguder et al., "Manifold learning for image-based gating of intravascular ultrasound (ivus) pullback sequences," in *Medical Imaging and Augmented Reality*. Springer, 2010, pp. 139–148.

[15] A. Hernàndez-Sabaté et al., "Image-based cardiac phase retrieval in intravascular ultrasound sequences," *IEEE Trans. Ultrason. Ferroelectrics Freq. Contr.*, vol. 58, no. 1, pp. 60–72, 2011.

[16] C. von Birgelen et al., "Electrocardiogram-gated intravascular ultrasound image acquisition after coronary stent deployment facilitates on-line three-dimensional reconstruction and automated lumen quantification." *J Am Coll Cardiol*, vol. 30, no. 2, pp. 436–443, 1997.

[17] C. von Birgelen et al., "Morphometric analysis in three-dimensional intracoronary ultrasound: an in vitro and in vivo study performed with a novel system for the contour detection of lumen and plaque." *Am. Heart. J.*, vol. 132, no. 3, pp. 516–527, 1996.

[18] J. G. Abbott and F. L. Thurstone, "Acoustic speckle: Theory and experimental analysis," *Ultrason. Imag.*, vol. 324, no. 4, pp. 303–324, 1979.

[19] L. D. Enochson and R. K. Otnes, *Programming and analysis for digital time series data*. Shock and Vibration Information Center [Washington], 1969.

[20] F. Harris, "On the use of windows for harmonic analysis with the discrete fourier transform," *Proceedings of the IEEE*, vol. 66, no. 1, pp. 51–83, 1978.